Controlling the Frequency of Macrocyclic Ring Rotation in Benzylic Amide [2]Catenanes

David A. Leigh,*,†,§ Aden Murphy,†,§ John P. Smart,† Michael S. Deleuze,‡ and Francesco Zerbetto*,‡

Contribution from the Department of Chemistry, University of Manchester Institute of Science and Technology (UMIST), Sackville St., Manchester M60 1QD, United Kingdom, and the Dipartimento di Chimica "G. Ciamician", Università degli Studi di Bologna, via F. Selmi 2, 40126 Bologna, Italy

Received December 1, 1997

Abstract: A combination of variable-temperature ^{1}H NMR spectroscopy and molecular mechanics calculations have been used to probe the factors that determine the rate of macrocyclic ring rotation in benzylic amide [2]catenanes. The results show that the interlocked macrocycle dynamics are governed by a delicate combination of steric effects, intricate inter-macrocyclic arrays of hydrogen bonds, $\pi-\pi$ stacking, and T herringbone-type interactions. A cascade of hydrogen-bond ruptures and formations is the principal event during circumvolution (complete rotation of one macrocyclic ring about the other) but is accompanied by a series of cooperative conformational and co-conformational rearrangements that help to stabilize the energy of the molecule. The experimental picture is consistent both when activation energies are measured from the coalescence of NMR signals and when rate constants are directly measured by spin polarization transfer by selective inversion recovery (SPT-SIR) methods. The nature of the circumrotational process means that the precise structure of the diacylaromatic units has a tremendous effect on the frequency of macrocyclic ring rotation: a 2,5-thiophene-based catenane rotates 3.2 million-fold faster than the analogous 2,6-pyridine-based system at room temperature! The polarity of the environment also plays a crucial role in determining the inter-ring dynamics: reducing the strength of the ground-state hydrogen-bonding network by employing hydrogen bond-disrupting solvents (methanol, DMSO) increases the rate of rotation by lowering the activation energy for circumvolution (normally in the region of 11−20 kcal mol^{-1}) by up to 3.2 kcal mol^{-1}. This allows exquisite control over the kinetics of the translational behavior of the individual components of an interlocked molecular system, a key requirement for their development as nanoscale shuttles, switches, and information storage systems.

Introduction

One of the most striking features of catenane and rotaxane architectures is that their mechanically interlocked components can, in principle, move relative to one another without breaking covalent bonds. Such dynamic processes are currently attracting considerable attention[1−3] from chemists, physicists, and materials scientists because they combine the possibility of precisely positioning the individual components of a molecule with that of changing their relative separation and orientation to order, possibly through the influence of external stimuli. Controlling the location of a macrocycle between two or more nonequivalent sites in a catenane or rotaxane has already been achieved as the first step in the development of nanoscale devices utilizing these novel architectures.[2,3] However, molecular machines based on catenanes and rotaxanes will be much more useful when the *rate* or *frequency* of their component translations or rotations are tunable through the judicious choice of their structure and operating environment.[3] Unfortunately, despite

† UMIST.

‡ Universitá degli Studi di Bologna.

§ Address from October 1, 1998: Department of Chemistry, University of Warwick, Coventry CV4 7AL, United Kingdom

(1) (a) de Silva, A. P.; McCoy, C. P. *Chem. Ind. (London)* **1994**, 992. (b) Drexler, K. E. *Annu. Rev. Biophys. Biomol. Struct.* **1994**, *23*, 377. (c) Whitesides, G. M. *Sci. Am.* **1995**, *273 (3)*, 114. (d) Ward, M. D. *Chem. Ind. (London)* **1997**, 640.

(2) (a) Anelli, P.-L.; Spencer, N.; Stoddart, J. F. *J. Am. Chem. Soc.* **1991**, *113*, 51313. (b) Ashton, P. R.; Bissell, R. A.; Spencer, N.; Stoddart, J. F.; Tolley, M. S. *Synlett* **1992**, 914. (c) Ashton, P. R.; Bissell, R. A.; Górski, R.; Philp, D.; Spencer, N.; Stoddart, J. F.; Tolley, M. S. *J. Am. Chem. Soc.* **1992**, 919. (d) Ashton, P. R.; Bissell, R. A.; Spencer, N.; Stoddart, J. F.; Tolley, M. S. *J. Am. Chem. Soc.* **1992**, 923. (e) Bissell, R. A.; Córdova, E.; Kaifer, A. E.; Stoddart, J. F. *Nature* **1994**, *369*, 133. (f) Benniston, A. C.; Harriman, A. *Angew. Chem., Int. Ed. Engl.* **1993**, *32*, 1459. (g) Benniston, A. C.; Harriman, A.; Lynch, V. M. *J. Am. Chem. Soc.* **1995**, *117*, 5275. (h) Benniston, A. C. *Chem. Soc. Rev.* **1996**, *25*, 427. (i) Ashton, P. R.; Ballardini, R.; Balzani, V.; Boyd, S. E.; Credi, A.; Gandolfi, M. T.; Gómez-López, M.; Iqbal, S.; Philp, D.; Preece, J. A.; Prodi, L.; Ricketts, H. G.; Stoddart, J. F.; Tolley, M. S.; Venturi, M.; White, A. J. P.; Williams, D. J. *Chem. Eur. J.* **1997**, *3*, 152. (j) Amabilino, D. B.; Sauvage, J.-P. *Chem. Commun.* **1996**, 2441. (k) Cárdenas, D. J.; Livoreil, A.; Sauvage, J.-P. *J. Am. Chem. Soc.* **1996**, *118*, 11980. (l) Baumann, F.; Livoreil, A.; Kaim, W.; Sauvage, J.-P. *Chem. Commun.* **1997**, 35. (m) Collin, J.-P.; Gavinã, P.; Sauvage, J.-P. *Chem. Commun.* **1996**, 2005. (n) Lane, A. S.; Leigh, D. A.; Murphy A. *J. Am. Chem. Soc.* **1997**, *119*, 11092.

(3) For catenanes where structure variations effect circumrotational dynamics, see: (a) Anelli, P.-L.; Ashton, P. R.; Ballardini, R.; Balzani, V.; Delgado, M.; Gandolfi, M. T.; Goodnow, T. T.; Kaifer, A. E.; Philp. D.; Pietraszkiewicz, M.; Prodi, L.; Reddington, M. V.; Slawin, A. M. Z.; Spencer, N.; Stoddart, J. F.; Vicent, C.; Williams, D. J. *J. Am. Chem. Soc.* **1992**, *114*, 193 and references therein. For catenanes where solvent variations effect circumrotational dynamics and translational isomerism, see: (b) Ashton, P. R.; Ballardini, R.; Balzani, V.; Credi, A.; Gandolfi, M. T.; Menzer, S.; Pérez-García, L.; Prodi, L.; Stoddart, J. F.; Venturi, M.; White, A. J. P.; Williams, D. J. *J. Am. Chem. Soc.* **1995**, *117*, 11171 and references therein. For leading references to chemical, electrochemical, and photochemical driven macrocyclic ring motions in catenanes, see: (c) Livoreil, A.; Sauvage, J.-P.; Armaroli, N.; Balzani, V.; Flamigni, L.; Ventura, B. *J. Am. Chem. Soc.* **1997**, *119*, 12114. (d) Asakawa, M.; Ashton, P. R.; Balzani, V.; Credi, A.; Hamers, C.; Mattersteig, G.; Montalti, M.; Shipway, A. N.; Spencer, N.; Stoddart, J. F.; Tolley, M. S.; Venturi, M.; White, A. J. P.; Williams, D. J. *Angew. Chem., Int. Ed. Engl.* **1998**, *37*, 333.

S0002-7863(97)04065-1 CCC: $15.00
Published on Web 06/20/1998

tremendous recent advances in the synthesis of catenanes and rotaxanes,[4] little is known about the mechanisms by which mechanically interlocked components move with respect to each other. Here we present the first study where experimentally determined energy barriers of macrocyclic ring rotation, one of the most interesting and important kind of dynamics found in catenane systems, are accurately simulated by theoretical modeling studies of the ring rotation mechanism for three significant examples of benzylic amide [2]catenanes.

Benzylic amide [2]catenanes[4e−g] are among the most accessible of interlocked molecules, most conveniently produced from the eight molecule condensations of 1,4-benzylic diamines and aromatic 1,3-dicarbonyl chlorides. The hydrogen bond-driven process responsible for their assembly is remarkably structurally tolerant and a diverse series of benzylic amide [2]catenanes has been produced, many of which exhibit qualitatively very different dynamic behavior. For example, the macrocyclic rings of some benzylic amide catenanes, e.g., **1** and **3**, rotate rapidly about one another at room temperature in polar solvents giving rise to relatively simple ^{1}H NMR spectra.[4e,f] In contrast, the rings of the pyridyl catenane **2** rotate only slowly on the NMR time scale below 100 °C and catenanes with substituents at the 5-position of the isophthaloyl unit, such as the methyl-substituted catenane **4**, are unable to undergo full circumvolution at all.[4f] We sought to explain the reasons for these fascinating differences in behavior by correlating experimental data for the rates of macrocyclic ring rotation (provided by variable-temperature NMR spectroscopy in both polar and relatively nonpolar solvents) with modeling studies.

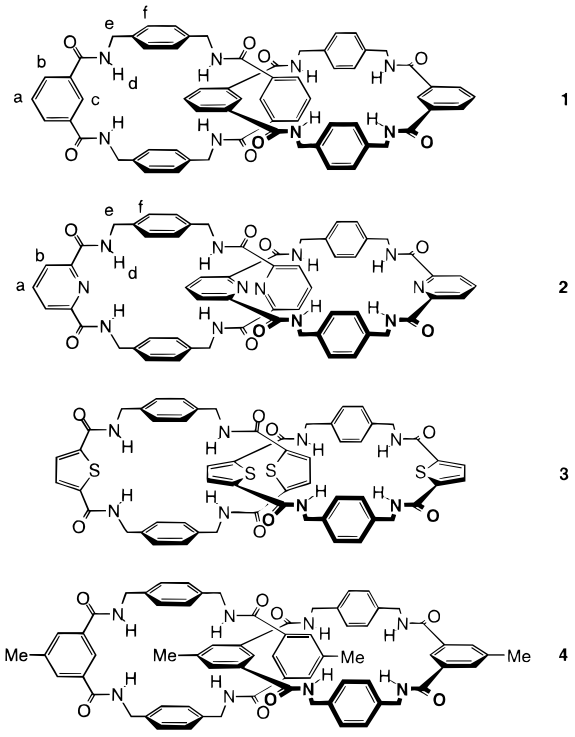

Experimental Measurement of Macrocyclic Ring Rotational Energy Barriers

The additional degrees of freedom inherent in catenane and rotaxane architectures include both the spinning of a macrocyclic ring about a fixed axis ("pirouetting") and the movement of a macrocycle between two or more points on a rotaxane or catenane thread ("shuttling", Figure 1). If a pirouetting or shuttling operation leads to the complete rotation of a particular

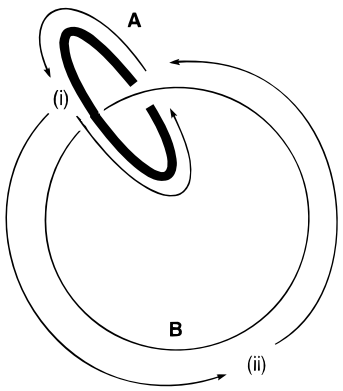

Figure 1. The two possible macrocyclic ring rotations that can occur in a [2]catenane architecture. For homocircuit catenanes, process i is identical to process ii; for heterocircuit catenanes, the two processes are different.

interlocked component it can properly be defined as a "circumrotational" or "circumvolutional" action. For the homocircuit (i.e., both rings are constitutionally the same) benzylic amide [2]catenanes **1**−**4** the shuttling and pirouetting processes are identical or energetically degenerate and can be conveniently thought of as comprising two separate site-exchange processes (types I and II) which must each occur at least twice during a single circumvolution event, as shown for **1** and **2** in Figure 2. The type I process is defined as the complete passing of a *p*-xylylene ring through the cavity of one macrocycle; the type II process is the passing of an aromatic 1,3-dicarbonyl unit.

To experimentally probe the dynamics of the benzylic amide catenane systems **1**−**3** (the energy barrier found for the type I process in **4** was the same, within experimental error, as that found for **1**; the type II process cannot occur) variable-temperature ^{1}H NMR spectra were acquired for each catenane in solvents that were anticipated to have either small or large effects on the intramolecular, intermacrocycle hydrogen bonding which dominates their solid-state structure and is the driving force for their formation.[4i] 1,1′,2,2′-Tetrachloroethane ($C_2D_2Cl_4$) proved the most convenient non-hydrogen bond-disrupting solvent to use because of the wide range of energy barriers involved ($C_2D_2Cl_4$ is liquid from 230 to 420 K at atmospheric pressure) and the generally good solubility of benzylic amide catenanes in this medium (where it was possible to obtain them, energy barriers measured in $CDCl_3$ or CD_2Cl_2 proved very similar to those measured in $C_2D_2Cl_4$). For hydrogen bond-disrupting solvents, the substrate solubilities—and the temperature ranges required—meant [D_6]DMSO (a particularly pow-

(4) (a) Schill, G. *Catenanes, Rotaxanes and Knots*; Academic Press: New York, 1971. (b) Amabilino, D. B.; Stoddart, J. F. *Chem. Rev.* **1995**, *95*, 2725. (c) Sauvage, J.-P. *Acc. Chem. Res.* **1990**, *23*, 319. (d) Gibson, H. W.; Bheda, M. C.; Engen, P. T. *Prog. Polym. Sci.* **1994**, *19*, 843. For octaamide benzylic amide catenanes, see: (e) Johnston, A. G.; Leigh, D. A.; Pritchard, R. J.; Deegan, M. D. *Angew. Chem., Int. Ed. Engl.* **1995**, *34*, 1209. (f) Johnston, A. G.; Leigh, D. A.; Nezhat, L.; Smart, J. P.; Deegan, M. D. *Angew. Chem., Int. Ed. Engl.* **1995**, *34*, 1212. For amphiphilic benzylic amide catenanes, see: (g) Leigh, D. A.; Moody, K.; Smart, J. P.; Watson, K. J.; Slawin, A. M. Z. *Angew. Chem., Int. Ed. Engl.* **1996**, *35*, 306. For benzylic amide rotaxanes, see: (h) Johnston, A. G.; Leigh, D. A.; Murphy, A.; Smart, J. P.; Deegan, M. D. *J. Am. Chem. Soc.* **1996**, *118*, 10662. (i) Leigh, D. A.; Murphy, A.; Smart, J. P.; Slawin, A. M. Z. *Angew. Chem., Int. Ed. Engl.* **1997,** *36*, 728. For a class of amide-based catenanes where the macrocyclic rings cannot circumrotate, see: (j) Hunter, C. A. *J. Am. Chem. Soc.* **1992**, *114*, 5303, (k) Vögtle, F.; Dunnwald, T.; Schmidt, T. *Acc. Chem. Res.* **1996**, *29*, 451.

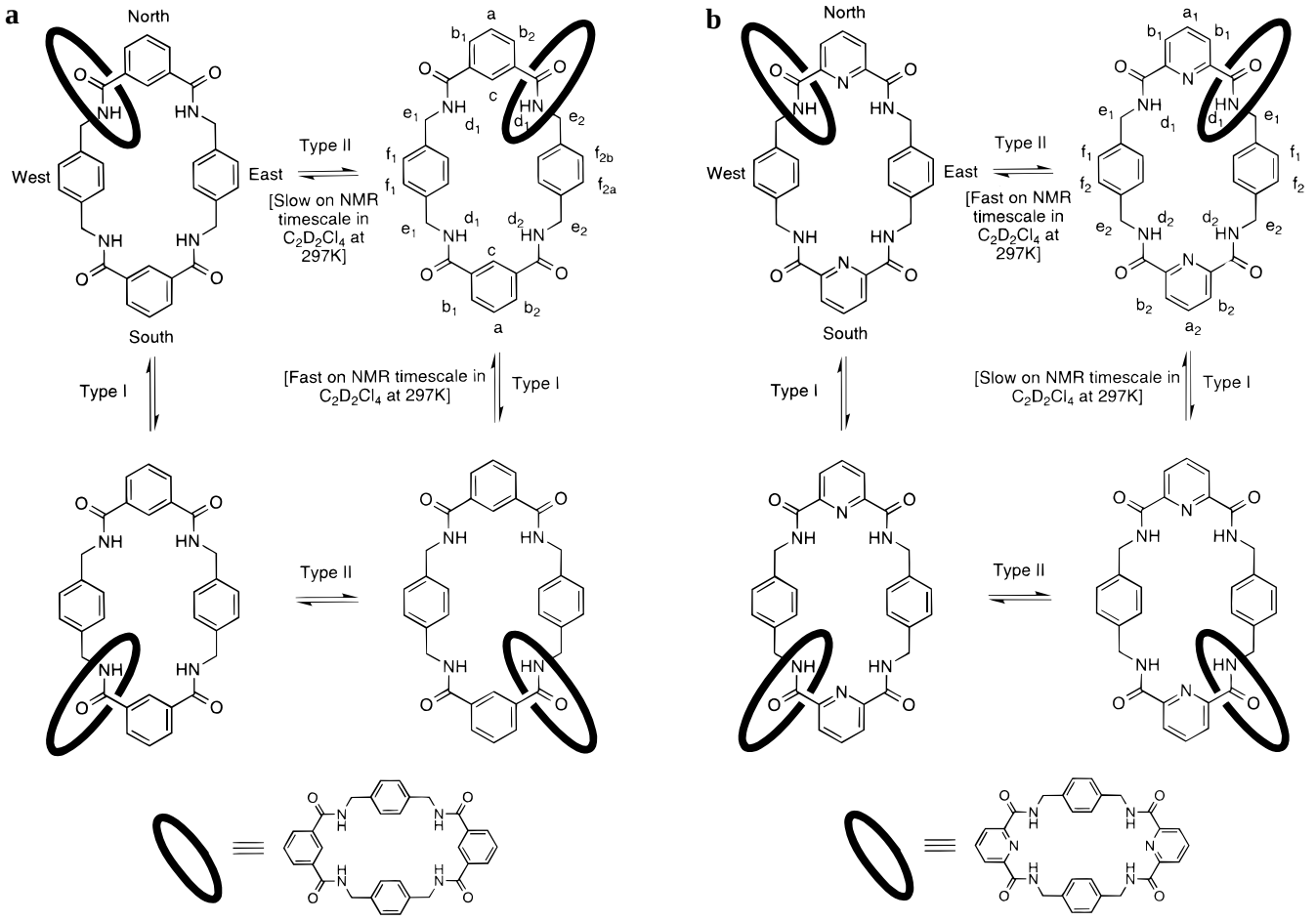

Figure 2. Site-exchange processes for macrocyclic ring circumvolution in homocircuit benzylic amide [2]catenanes (a) **1** and (b) **2**.

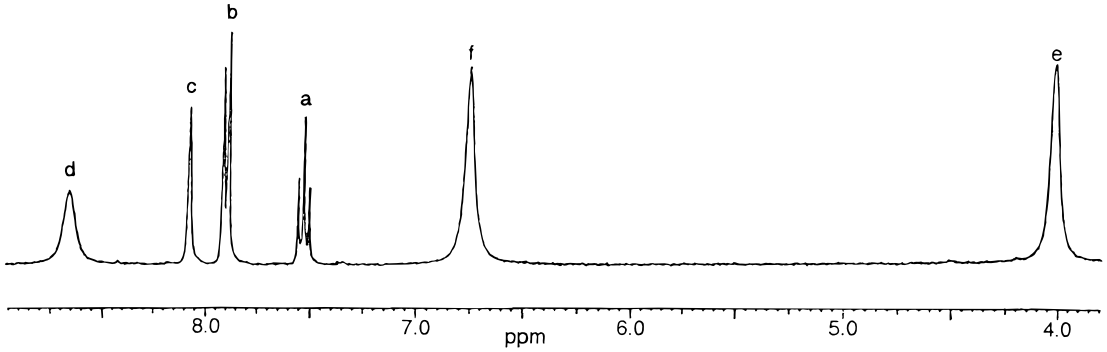

Figure 3. ^{1}H NMR spectrum (300 MHz) of **1** in [D_6]DMSO at 297 K.

erful hydrogen bond-accepting solvent[5]) was used for processes with coalescence temperatures greater than room temperature, while CD_3OD was used to measure energy barriers below the freezing point of DMSO (291 K).

Dynamic ^{1}H NMR Spectroscopy. For the original benzylic amide [2]catenane, **1**, an indication of the importance of intercomponent hydrogen bonding on the dynamics of macrocyclic ring rotation is evident merely from inspection of the room temperature ^{1}H NMR spectra in the two different types of solvent systems. The 297K ^{1}H NMR spectrum of **1** in [D_6]-DMSO (Figure 3) contains the minimum number of signals possible (e.g., all 16 xylylene aromatic protons, H_f, appear as a singlet) indicating that both type I and II processes, and other inter- and intracomponent conformational, co-conformational,[6] and hydrogen-bonding motif interconversions, are rapid on the NMR time scale under these conditions. In contrast, in $C_2D_2Cl_4$ at 297 K (Figure 4, spectrum [B]) the resonances of **1** are generally much broader and *two* sets of signals are observed for the xylylene ring protons (H_{f1} and H_{f2}) and benzylic methylene protons (H_{e1} and H_{e2}), indicating that now either the type I or type II exchange process is slow on the NMR time scale. In fact, since there is only one resonance in spectrum [B] for H_a, which lies on the "north−south" axis, the slower (i.e., higher energy barrier) process in this case must be type II. This is confirmed by ^{1}H,^{1}H-COSY experiments that show

(5) Arnett, E. M.; Mitchell, E. J.; Murty, T. S. S. R. *J. Am. Chem. Soc.* **1974**, *96*, 3875.

(6) "Co-conformation" refers to the relative positions and orientations of the mechanically interlocked components with respect to each other (Fyfe, M. C. T.; Glink, P. T.; Menzer, S.; Stoddart, J. F.; White, A. J. P.; Williams, D. J. *Angew. Chem., Int. Ed. Engl.* **1997**, *36*, 2068).

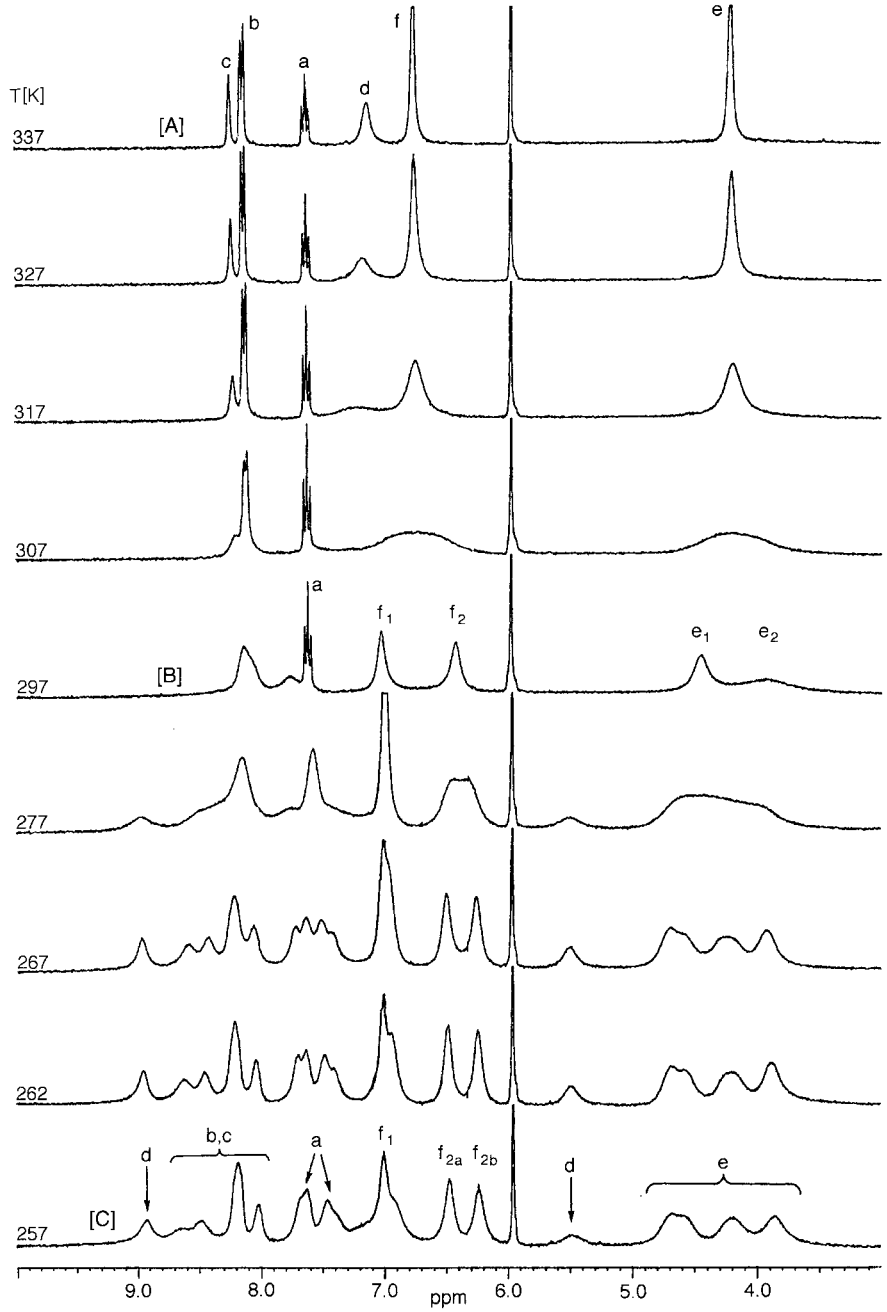

Figure 4. ^{1}H NMR spectra (300 MHz) of **1** in $C_2D_2Cl_4$ at 337 K (A), 297 K (B), and 257 K (C).

that the resolved H_{f1} and H_{f2} resonances are not coupled to each other (they would be coupled if it were the "north−south" ends of the macrocycles that were nonequivalent, cf. **2** in Figures 2a and 5). Furthermore, the H_{f1} and H_{f2} resonances can be assigned as the "west" and "east" xylylene rings, respectively, since in the absence of type II processes only the west half of the macrocycle experiences shielding effects from the enveloping macrocycle (cf. the ^{1}H NMR spectrum of the methyl-substituted catenane **4**[4f]).

Significant differences between the room-temperature $C_2D_2Cl_4$ ^{1}H NMR spectra of catenanes **1** (Figure 4, spectrum B) and **2** (Figure 5) reveal that the structure of the diacylaromatic unit of a benzylic amide catenane has a major effect on the pathway adopted for the macrocyclic ring rotation process. In contrast to **1**, *two* sets of resonances are observed for the H_a protons (H_{a1} and H_{a2}) of **2** and the xylyl ring resonances (H_{f1} and H_{f2}) appear as an AA′BB′ system indicating that the east−west halves of each macrocycle are in fast exchange at 297 K whereas the north−south ends are not−i.e., the type I process in **2** is slower than the type II process!

Heating of **1** to 337 K in $C_2D_2Cl_4$ causes the ^{1}H NMR spectrum (Figure 4, spectrum A) of **1** to become as simple as the room-temperature spectrum (Figure 3) in [D_6]DMSO, i.e., the type II exchange becomes rapid on the NMR time scale. The energy barrier for the type II process of **1** in $C_2D_2Cl_4$, can be calculated[7] from the coalescence temperature and the limiting chemical shift difference of the H_f protons to be 14.5 kcal mol^{-1} at 307K (Table 2). Cooling to 257 K (Figure 4, spectrum [C]) leads to freezing out of the type I process. At this temperature the H_{f2} resonances of **1** are resolved into two distinct signals (H_{f2a} and H_{f2b}) which ^{1}H,^{1}H-COSY experiments confirm are coupled. However, it is evident from Figure 4 that other dynamic conformational and/or co-conformational interconversions are also becoming slow on the NMR time scale at this

(7) (a) Sutherland, I. O. *Annu. Rep. NMR Spectrosc.* **1971**, *4*, 71. (b) Sandström, J. *Dynamic NMR Spectroscopy*; Academic Press: London, 1982.

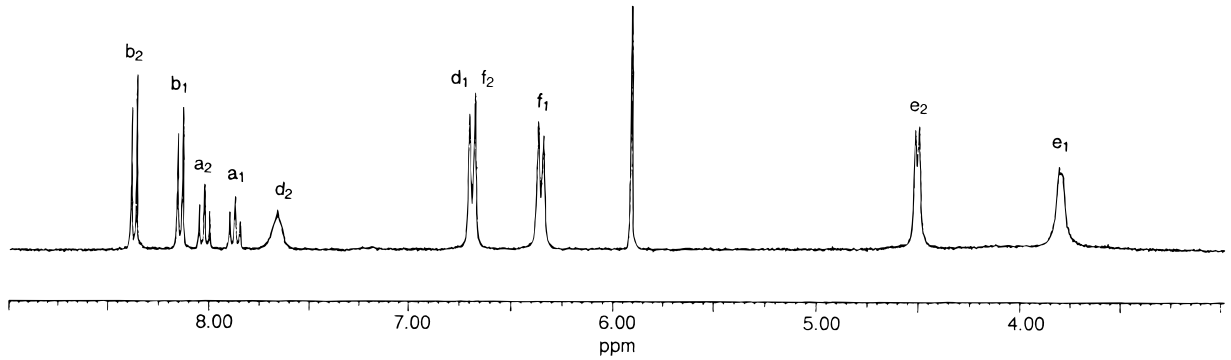

Figure 5. ^{1}H NMR spectrum (300 MHz) of **2** in $C_2D_2Cl_4$ at 297 K.

temperature and the precise coalescence temperatures for various signals are difficult to determine accurately, as are the limiting chemical shift differences in slow exchange regimes. Quantitative information about the differences in the rates of macrocyclic ring rotation for **1**−**3** were thus obtained using a combination of coalescence temperature measurements and dynamic spin polarization transfer by selective inverse recovery (SPT-SIR)[8] experiments.

The SPT-SIR Technique. The rates (k) and energy barriers of shuttling and spinning processes in interlocked systems have previously[2,3] only been measured experimentally by the standard NMR coalescence method,[7] which gives the rate of interconversion between two states at the coalescence temperature (T_c) of the signals, or by simulation[7] of the line shape of the exchanging signals close to T_c. However, both these methods have practical and theoretical limitations associated with them. The determination of T_c is inherently subjective and often difficult if the signals are even partially obscured or well-separated (for example, where aromatic shielding of a proton is involved in one state but not in the other). Furthermore, variable-temperature broadening of signals occurs for many reasons other than the rate of site exchange including solvent viscosity changes over the temperature range, poor shimming, temperature variation through the sample, precipitation at low temperatures, aggregation effects, and, as described above for **1**, the slowing down of other structural and conformational exchange processes in the molecule. In the case of benzylic amide catenanes, this last complication includes both chair−chair and chair−boat/twist boat conformational interconversions of each macrocycle along with the interchange between different intercomponent hydrogen bonding motifs.

An alternative NMR method for directly determining the rates of dynamic processes is proton SPT-SIR[8] which has none of the disadvantages listed above but must be carried out at temperatures where the proton resonances for the two sites are resolved, i.e., in slow exchange. At temperatures where site exchange lifetimes, τ, are of the same order of magnitude as the longitudinal relaxation times of the nuclei, k (τ^{-1}) can be conveniently and accurately determined by selective inversion of the signal due to the nuclei at one site with a soft 180° pulse leading to a corresponding loss of intensity of the signal due to the nuclei at the other site dependent on their rate of exchange.

(8) (a) Dahlquist, F. W.; Longmur, K. J.; Du Vernet, R. B. *J. Magn. Reson.* **1975**, *17*, 406. For recent examples, see: (b) Ben-David Blanca, M.; Maimon, E.; Kost, D. *Angew. Chem., Int. Ed. Engl.* **1997**, *36*, 2216. (c) Kelly, T. R.; Tellitu, I.; Sestelo, J. P. *Angew. Chem., Int. Ed. Engl.* **1997**, *36*, 1866. (d) Abdourazak, A. H.; Sygula, S.; Rabideau, P. W. *J. Am. Chem. Soc.* **1993**, *115*, 3010. (e) Frim, R.; Zilber, G.; Rabinovitz, M. *J. Chem. Soc., Chem. Commun.* **1991**, 1202. For a review of 2D methods for determining the kinetics of exchange processes, see: (f) Perrin, C. L.; Dwyer, T. J. *Chem. Rev.* **1990**, *90*, 935.

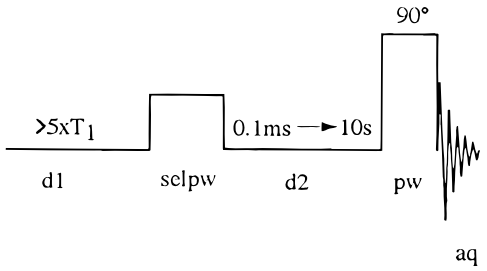

Figure 6. Pulse sequence for spin polarization transfer by selective inversion recovery (SPT-SIR) NMR experiments. d1 = initial delay; selpw = soft selective inversion (180°) pulse for ≫1/difference in frequency of the exchanging signals; d2 = variable delay encompassing the time frame of signal exchange; pw = hard 90° pulse; aq = acquisition.

Correlating the loss of signal intensity at the nonirradiated site over time allows calculation of τ and thus k at a given temperature. Since only a relative loss of intensity is measured it does not matter if one of the two exchanging resonances is obscured, or even if both are unless the overlapping resonances are themselves exchanging on a similar time scale. SPT-SIR can even be carried out on systems where the coalescence temperature cannot actually be reached (e.g., **2** in $C_2D_2Cl_4$). A further advantage is that since SPT-SIR can be achieved over a range of temperatures for a molecule, both ΔH and ΔS of spinning or shuttling processes can also be conveniently and accurately calculated by this method. (Previously ΔH and ΔS have been measured by carrying out coalescence measurements at different field strengths or line shape analysis.)

The SPT-SIR experiments were performed on catenanes **1**−**3** with the pulse sequence outlined in Figure 6 at a range of temperatures where the signals for two sites were in slow exchange (for example, H_{f1} and H_{f2} in Figure 4, spectrum B, to determine k for the type II process for **1** in $C_2D_2Cl_4$ at 297 K).

After an initial delay (d1) of $>5\times T_1$ of the observed nuclei, a soft 180° pulse (selpw) was applied for $\gg 1/\Delta f$ (Δf = frequency difference between the two sites) seconds to one of the exchanging sites (e.g., H_{f1}). A delay (d2) allowed exchange of the sites after which a hard 90° pulse (pw) was applied to acquire the complete spectrum. By varying d2 over a range (typically from 1ms to 10s) whose limits were short and long with respect to the site exchange lifetime, a series of spectra were collected where the intensity, I, of the signal for the nonirradiated site varied (e.g., Table 1) according to the rate of site exchange and T_1 by the biexponential function (which holds when $\tau \ll T_1$):

$$I(t) = I_\infty - Y\exp(-t/\tau) + Z\exp(-t/T_1) \qquad (1)$$

where $I(t)$ is the signal intensity at time t in seconds, I_∞ is the signal intensity for $d_2 = \infty$, and Y and Z are constants.

Table 1. Experimental Data[a] for the Direct Determination of k for the Type II Process of **1** in $C_2D_2Cl_4$ at 297 K by Selective Inversion Recovery of H_{f1}

d_2, s	I(observed)	I(calculated)	difference
0.0001	18.59	18.55	0.042
0.0002	18.24	18.29	−0.045
0.0005	17.51	17.52	−0.008
0.001	16.31	16.32	−0.006
0.002	14.18	14.17	0.009
0.005	9.41	9.39	0.02
0.01	5.01	5.02	−0.01
0.02	2.07	2.12	−0.05
0.005	1.74	1.84	−0.1
0.1	2.75	2.77	−0.02
0.2	4.60	4.53	0.07
0.5	9.16	9.02	0.14
1	14.42	14.37	0.05
2	19.98	20.17	−0.19
5	24.12	24.19	−0.07
10	24.66	24.53	0.13

[a] I(observed) = observed intensity of H_{f2}. I(calculated) = intensity of H_{f2} calculated from $I(t) = I_\infty - Y\exp(-t/\tau) + Z\exp(-t/T_1)$ with the best-fit parameters $I_\infty = 24.53$; $Y = 17.97$; $\tau = 0.0066$; $Z = -23.68$; $T_1 = 1.2$. Error in data fitting of $\tau = \pm 0.00009$. $k_{297} = 151 \pm 3\ s^{-1}$.

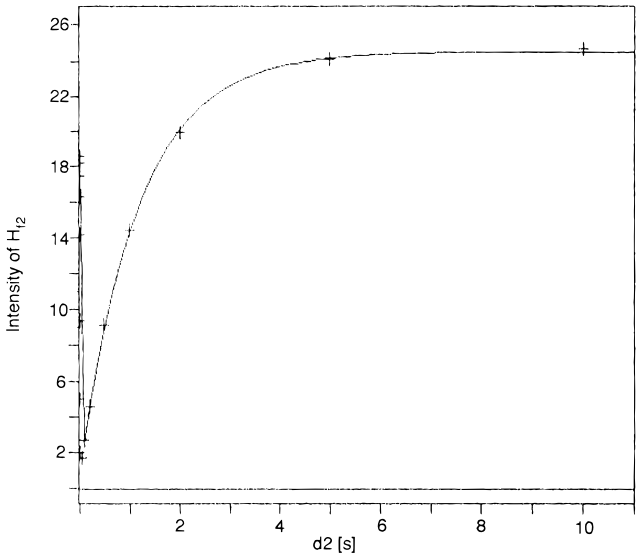

Figure 7. Five parameter biexponential fit for the experimental data (Table 1) for the direct determination of k for the type II process of **1** in $C_2D_2Cl_4$ at 297 K by SPT-SIR of H_{f1}.

τ, and hence k, was obtained by fitting (e.g., Table 1 and Figure 7) the observed intensities of the nonirradiated peak to the five parameter biexponential eq 1.

Having established k directly (SPT-SIR) or indirectly (from coalescence measurements) for the resolvable type I and II processes for catenanes **1**−**3** in both types of solvent, energy barriers were estimated using an extrapolation (eq 2) of the Eyring equation which assumes that all of the molecules reaching the exchange process transition state cross to the other side:[7]

$$\Delta G^{\ddagger} = aT[10.319 + \log(T/k)] \qquad (2)$$

where $a = 4.575 \times 10^{-3}$ (for $\Delta G^{\ddagger}$ in kcal mol^{-1}).

To provide a common framework for comparing the dynamics of the different catenanes and different solvent types, the same equation was used to estimate circumvolution rates at 298 K, under the assumption that this energy barrier is rate determining and is passed twice in a single circumvolution event. The results of both coalescence and SPT-SIR NMR experiments are summarized in Tables 2−4. The errors in the absolute values of $\Delta G^{\ddagger}$ are estimated at ±0.2 kcal mol^{-1} and include approximations inherent in the Eyring equation, instrumentation and, where used, the NMR method of coalescence. Errors in the relative values of $\Delta G^{\ddagger}$ (e.g., the differences between $\Delta G^{\ddagger}$

Table 2

catenane	solvent	process	$\Delta G^{\ddagger}_T$, kcal mol^{-1}	T, K	$\Delta G^{\ddagger}_{298}$ kcal mol^{-1}	frequency, Hz of circmvolution at 298 K
isophth **1**	$C_2D_2Cl_4$	I	12.3[a]	280	12.3	72
			12.26[b]	258		
			12.27[b]	253		
			12.28[b]	248		
			12.22[b]	243		
isophth **1**	$C_2D_2Cl_4$	II	14.5[a]	307	14.5	
			14.47[b]	297		
			14.47[b]	293		
			14.48[b]	288		
			14.48[b]	283		
isophth **1**	CD_3OD	I	*c*			16 000
Isophth **1**	CD_3OD[d]	II	11.33[b]	233	11.3	
			11.34[b]	230		
			11.31[b]	228		
			11.28[b]	225		

[a] Calculated by coalescence measurements. [b] Calculated by SPT-SIR. [c] $\Delta G^{\ddagger}$ too low to measure because of insolubility of substrate at low temperatures. [d] Similar values of $\Delta G^{\ddagger}$ were obtained with a solvent mixture of 10%CD_3OD and 90%$CDCl_3$ or $C_2D_2Cl_4$.

Table 3

catenane	solvent	process	$\Delta G^{\ddagger}_T$, kcal mol^{-1}	T, K	$\Delta G^{\ddagger}_{298}$, kcal mol^{-1}	frequency, (Hz) of circmvolution at 298 K
pyridyl **2**	$C_2D_2Cl_4$	II	11.33[b]	238	**11.3**	0.003
			11.35[b]	235		
			11.39[b]	233		
			11.31[b]	230		
pyridyl **2**	$C_2D_2Cl_4$	I	20.50[b]	373	**20.5**	
			20.46[b]	368		
			20.61[b]	363		
			20.52[b]	360		
pyridyl **2**	[D_6]DMSO	II	*c*			0.2
pyridyl **2**	[D_6]DMSO	I	17.9[a]	373	17.9	
			18.05[b]	363		
			17.95[b]	358		
			17.88[b]	353		
			17.85[b]	343		
			17.85[b]	340		

[a,b] See Table 2. [c] $\Delta G^{\ddagger}$ too low to measure because of freezing point of solvent.

Table 4

catenane	solvent	process	$\Delta G^{\ddagger}_T$, kcal mol^{-1}	T, K	$\Delta G^{\ddagger}_{298}$, kcal mol^{-1}	frequency, (Hz) of circmvolution at 298 K
thioph **3**	$C_2D_2Cl_4$	II	*a*			9 600
thioph **3**	$C_2D_2Cl_4$	I	11.65[b]	230	**11.6**	
			11.63[b]	225		
			11.62[b]	222		
			11.62[b]	220		
thioph **3**	CD_3OD	II	*c*			28 000
thioph **3**	CD_3OD[d]	I	10.95[b]	210	**11.0**	
			11.03[b]	207		
			10.97[b]	203		
			10.93[b]	200		

[a] See footnote *c*, Table 3. [b] See footnote *b*, Table 2. [c] See footnote *c*, Table 2.

for **1**, **2**, and **3** in particular solvents or the decreases in $\Delta G^{\ddagger}$ upon addition of CD_3OD to a $C_2D_2Cl_4$ solution) are certainly much smaller, particularly when based on *k* measured by SPT-SIR (as shown by the error treatment of the experimental data in Table 1), and overall are estimated at ± 0.1 kcal mol^{-1}.

Rates of Circumrotation. The results outlined in Tables 2−4 confirm quantitatively that benzylic amide catenanes as a class exhibit truly extraordinary structure-dependent dynamic behavior. In $C_2D_2Cl_4$, the macrocyclic rings of the thiophene-based catenane **3** rotate 3.2 million times faster (9600 compared with 0.003 Hz) at room temperature than the pyridine analogue **2**! Having such a wide time scale available for dynamic processes augurs well for "designing in" the particular operating frequency required for using these types of mechanically interlocked subunits in nanoscale devices. Some of the key reasons behind these remarkable variations in dynamic properties were elucidated through modeling studies and are discussed in the following section.

The differences between the rotational energy barriers in polar and nonpolar solvents illustrate that in addition to varying the catenane structure, the nature of the local environment can be used to "fine-tune" energy barriers and therefore allow even greater control over circumvolution rates. A 3.2 kcal mol^{-1} decrease in $\Delta G^{\ddagger}$ is observed (a 220-fold circumvolution frequency increase at 298 K) for **1** when changing solvent from $C_2D_2Cl_4$ to CD_3OD. *However, the same reduction in activation energy can be achieved using a 9:1 $C_2D_2Cl_4$/CD_3OD mixture!* Accordingly, the room temperature (for example) rates of circumvolution of **1** can be chosen to be any value between 72 and 16 000 Hz by controlling the concentration (0−10%) of CD_3OD added to a solution of **1** in $C_2D_2Cl_4$. This appears to be a powerful general method for controlling the dynamics of benzylic amide catenanes since similar trends (albeit over slightly smaller frequency ranges) are seen for catenanes **2** and **3** and in peptide-based molecular shuttles.[2n]

Modeling the Circumrotational Process

As demonstrated by the ^{1}H NMR energy barrier measurements in different types of solvent, the principal events surrounding the circumrotational process entails hydrogen bond breaking and formation. Because of the flexible nature of the catenanes, the molecules can readily rearrange to create other weakly binding interactions. The circumrotation must therefore occur as a cooperative process of assembly and disassembly of hydrogen bonds (be they normal or bifurcated), π-stacking interactions, and phenyl−phenyl T-shaped herringbone interactions. The exponential increase in the number of variables to consider requires a computational approach able to unravel the complex features of such a dynamic system. Molecular mechanics is particularly well-suited for this sort of problem. Two possible treatments come to mind: the first is to run a molecular dynamics simulation of the catenanes where circumrotation would appear as a "rare event". The second is to explore the potential energy surface in terms of stationary points, local energy minima, and transition states. The calculated energy barriers (plus the zero point energies) would then correspond to the enthalpic contribution of the conformational and co-conformational modifications. We favored this second approach despite the considerable difficulty in dealing in a systematic way with the very large number of stationary points of the co-conformational potential energy surface of these molecules. The calculations were performed with the TINKER suite of programs[9] using the MM3 force field.[10,11] The choice of the force field was made because of its widespread use that has made it a standard complementary tool of experimental work. As usual, the synergy with the experimental results is the best criterion by which to judge the accuracy of the method. Location of the stationary points comes with the important advantages of (i) being able to depict the structure of the molecule when it passes through the (highest) barriers along the circumrotation pathway and (ii) being able to represent the infinitesimal motion responsible for the circumrotation at the top of the barrier(s). The combination of the two pictures affords genuine physical insight into the circumvolutional motion of the interlocked macrocyclic rings and the factors that govern the process.

The calculations reported here are for isolated molecules, the inclusion of polarization and viscosity effects was not attempted. The results are, accordingly, best compared with the NMR data obtained in apolar solvents. We emphasize that the present simulations have only a qualitative or semiquantitative value, but it is expected that while some of the energies of the transition states may be affected by factors not considered in this treatment, the geometrical nature of the passing through of the aromatic 1,3-dicarbonyl and the *p*-xylyl units will remain essentially the same since they are mainly governed by intramolecular, intermacrocycle interactions.

The NMR studies of **1**−**3** prove that site-exchange between the various interchangeable protons occurs with specific associated energy barriers. In all three cases the complete circumvolution of a macrocyclic ring is accomplished in (at least) four steps (Figure 2a,b). Each step has its own barrier which, to a first approximation, is likely to be due to the bulkiest groups of a fragment that passes through the cavity of the other macrocycle. Since the X-ray structure of the isophthaloyl catenane (**1**) was available,[4e] a series of rigid rotations was applied to the coordinates of one of the two macrocycles.[12] The molecular geometries generated in this way were then optimized with the aim of locating energy minima and transition states.[13] The transitions states for the threading through of the two different phenyl units were located and subjected to a shake up procedure to ensure that they corresponded to the lowest energy transition states. In Table 5, the characteristics of such states are summarized for the isophthaloyl (**1**), pyridyl (**2**), and thiophenyl (**3**) catenanes. The $\Delta G^{\ddagger}$ is obtained with the entropic factor calculated in the harmonic approximation.

The modeling results obtained are in good-to-excellent agreement with the experimental NMR data. The strong effect on the barrier to the passage of the *p*-xylyl group upon substitution of the phenyl group of the isophthaloyl moiety by a pyridine ring is particularly well simulated. Also the decrease of the activation energies for the circumvolution of the thiophene catenane is well-reproduced. Only partial agreement is found for the pyridyl catenane: the larger barrier is predicted ac-

(9) (a) Dudek, M.; Ponder, J. *J. Comput. Chem.* **1995**, *16*, 791. (b) Kundrot, C.; Ponder, J.; Richards, F. *J. Comput. Chem.* **1991**, *12*, 402. (c) Ponder, J.; Richards, F. *J. Comput. Chem.* **1987**, *8*, 1016.

(10) (a) Allinger, N. L.; Yuh, Y. H.; Lii, J.-H. *J. Am. Chem. Soc.* **1989**, *111*, 8551. (b) Lii, J.-H.; Allinger, N. L. *J. Am. Chem. Soc.* **1989**, *111*, 8566. (c) Lii, J.-H.; Allinger, N. L. *J. Am. Chem. Soc.* **1989**, *111*, 8576.

(11) Some of the required parameters of the MM3 force field (e.g., the bending and torsional energy contributions arising from conjugated amide groups) were not available from commercial or public domain sources and were extrapolated from similar, parametrized functional group types.

(12) Deleuze, M. S.; Leigh, D. A.; Zerbetto, F. Manuscript in preparation. In this paper a full description of the many minima energy structures and transition states of the benzylic amide catenanes will be given along with full details of the modeling methods.

(13) For the purposes of this study, a transition state is defined as a point on the potential energy surface whose energy gradient with respect to nuclear displacements is zero and whose Hessian matrix is characterized by only one negative eigenvalue.

Table 5. MM3 Characterization of the Transition States for the Passing of Various Groups in the Circumrotation of the Isophthaloyl (**1**), Pyridyl (**2**), and Thiophenyl (3) Catenanes

catenane	process	$\Delta E^{\ddagger}$, kcal mol^{-1}	$\Delta H^{\ddagger}$, kcal mol^{-1}	$\Delta S^{\ddagger}$, cal	$\Delta G^{\ddagger}_{298}$,[a] kcal mol^{-1}	transition state imaginary frequency, cm^{-1}
isophth **1**	I	12.1	10.6	−6.5	12.6 (12.3)	19
isophth **1**	II	14.4	13.7	−4.6	15.1 (14.5)	19
pyridyl **2**	I	18.6	17.6	−9.8	20.5 (20.5)	31
pyridyl **2**	II	14.8	14.1	−12.7	17.9 (11.3)	17
thioph **3**	I	12.0	11.1	1.9	10.5 (11.6)	11
thioph **3**	II	5.3	5.0	−12.1	8.6 (−)	33
	II	5.4	4.7	−1.5	4.2 (−)	34
	II	5.4	5.3	−0.2	5.2 (−)	38

[a] The experimental value in $C_2D_2Cl_4$ (from Tables 2−4) is given in parentheses.

curately, but the second barrier is overestimated by 6.6 kcal mol^{-1}. This result, along with its very strong entropic contribution, makes us believe that, in contrast to the other five transition states, solvent effects—not included in the simulations—may be very important in the energetics for this site exchange.

The simulations provide the description of the molecular shape at the transition states which are shown in Figure 8 together with the nuclear displacement that triggers the catenane rearrangement toward the minima. Some features of the transition states are immediately evident, others are more difficult to visualize using this two-dimensional representation (the coordinates of the structures are provided as Supporting Information), and the following features are of particular interest:

(i) The geometry (Figure 8a) of the transition state for the passage of a *p*-xylyl unit of one (yellow) macrocycle of catenane **1** inside the cavity of the other (green) macrocycle is characterized by one fewer pair of bifurcated hydrogen bonds than the X-ray structure (Figure 9a). However, the *p*-xylyl fragment forms a phenyl−phenyl T-shaped interaction with the H_c hydrogen of an isophthaloyl group of the other macrocycle which helps to reduce the energy of this structure. This arrangement leads us to call this type of transition state "perpendicular". A further stabilizing interaction is due to one of the two pairs of π-stacks of the X-ray structure that is now upgraded to a π-electron triple decker sandwich (labeled "$\pi-\pi-\pi$" in Figure 8a).

(ii) From the structure of the transition state shown in Figure 8b, it can be seen that the passage of an isophthaloyl unit of **1** also occurs via a π-electron triple decker sandwich, an arrangement which directly reduces the steric interactions as well as contributing some additional $\pi-\pi$ stabilizing interactions leading us to define it as a "parallel" transition state. This transition state has only four hydrogen bonds and has lost a pair of bifurcated hydrogen bonds that were present in the X-ray structure.

(iii) The low-energy co-conformer utilized (Figure 9b) for the pyridyl catenane **2** is slightly but significantly different from the X-ray structure of the isophthaloyl catenane (**1**), the principal change being that one of the pyridyl macrocycles has an additional *endo* (to the macrocyclic cavity) NH bond rotamer. This allows both an additional N(pyr)···H—N bridge and three pairs of bifurcated hydrogen bonds instead of the two regular and the two pairs of bifurcated hydrogen bonds found in the X-ray structure of **1**. In general, the transition states of the pyridyl catenane (Figure 8c,d) still closely resemble those of its isophthaloyl analogue. The large energy difference between the passing of the respective *p*-xylyl moieties arises from (a) substituting the phenyl−phenyl T-shaped interaction with the interaction between a nitrogen atom with the core of a phenyl group (both of which have a negative charge leading to a destabilization that is reflected in the dramatically warped shape of the phenyl group in **2**), (b) because the additional *endo* NH bond reverts to the *exo* rotamer in the transition state thereby breaking the third N(pyr)···H—N bridge, and (c) because the balance of the hydrogen-bonding contribution in **2** is shifted to one pair of bifurcated hydrogen bonds and two regular hydrogen bonds in the transition state.

(iv) The transition state for the passing through of the pyridyl fragment (Figure 8d) is "parallel" as in the case of the type II process in **1**. It has two pairs of bifurcated hydrogen bonds and one regular hydrogen bond and the same number of N(pyr)···H—N bridges as the low-energy structure (Figure 9b).

(v) The low-energy structure of **3** is relatively poor in hydrogen bonds compared to those of **1** and **2** and contains only four O···H—N regular hydrogen bonds. The transition state for the passing through of the *p*-xylyl unit (Figure 8e) is similar to that of **1** (Figure 8a), i.e., through a "perpendicular" arrangement. The strength of the interactions is now decreased by the smaller size of the five-membered thiophene ring which allows the system to release some steric constraints and avoids the possible insurgence of repulsion between a negatively polarized S atom and the negatively polarized core of the passing phenyl ring.

(vi) The transition state for the passing of the thiophene unit (Figure 8f) is calculated to be much lower than all the others. This is a consequence of the increased flexibility of this macrocyclic ring system which is also reflected in that more than one transition state is found for this site exchange. A unifying feature of all these transition states, however, is that they resemble the global energy minimum (Figure 9c) with a stack of four parallel thiophene rings (labeled "$\pi-\pi-\pi-\pi$" in Figure 8f).

Two further points are worth emphasizing: the first is that benzylic amide catenane circumrotation is a highly concerted process that occurs via the disruption and partial reconstruction of their intricate hydrogen bonding networks. To accommodate this the catenanes resort to a number of expedients entailing the transient formation of π-stacking interactions, phenyl−phenyl T-shaped interactions and amide bond rotamerization which reduces considerably the energy required for the rotational process. The second point is that the spatial (re)arrangements of the atoms in each transition state furnish a simple explanation for the large variation in dynamic behavior observed experimentally through the NMR experiments. In particular, the increase in the barrier (from the isophthaloyl to the pyridyl catenane) for the passage of the *p*-xylyl unit is caused by the combined effect of depriving the system of a binding phenyl−phenyl T-shaped interaction and replacing it with the interaction between two negatively polarized centers, plus a steric constraint that forces the rotamerization of a NH group from *endo* to *exo* by breaking a positive (hydrogen bonding) interaction in the pyridyl catenane.

Overall, the theoretically determined activation barriers compare extremely well with those determined experimentally. Although, the full exploration of the potential energy surface and dynamics of the circumrotation is still in progress,[12] the present results lead us to believe that we have captured the essence of benzylic amide catenane circumvolution.

Conclusions

Solvent effects and structural modifications can induce large variations in the rate of circumrotation of benzylic amide catenanes [which can range from the sub-microsecond time scale

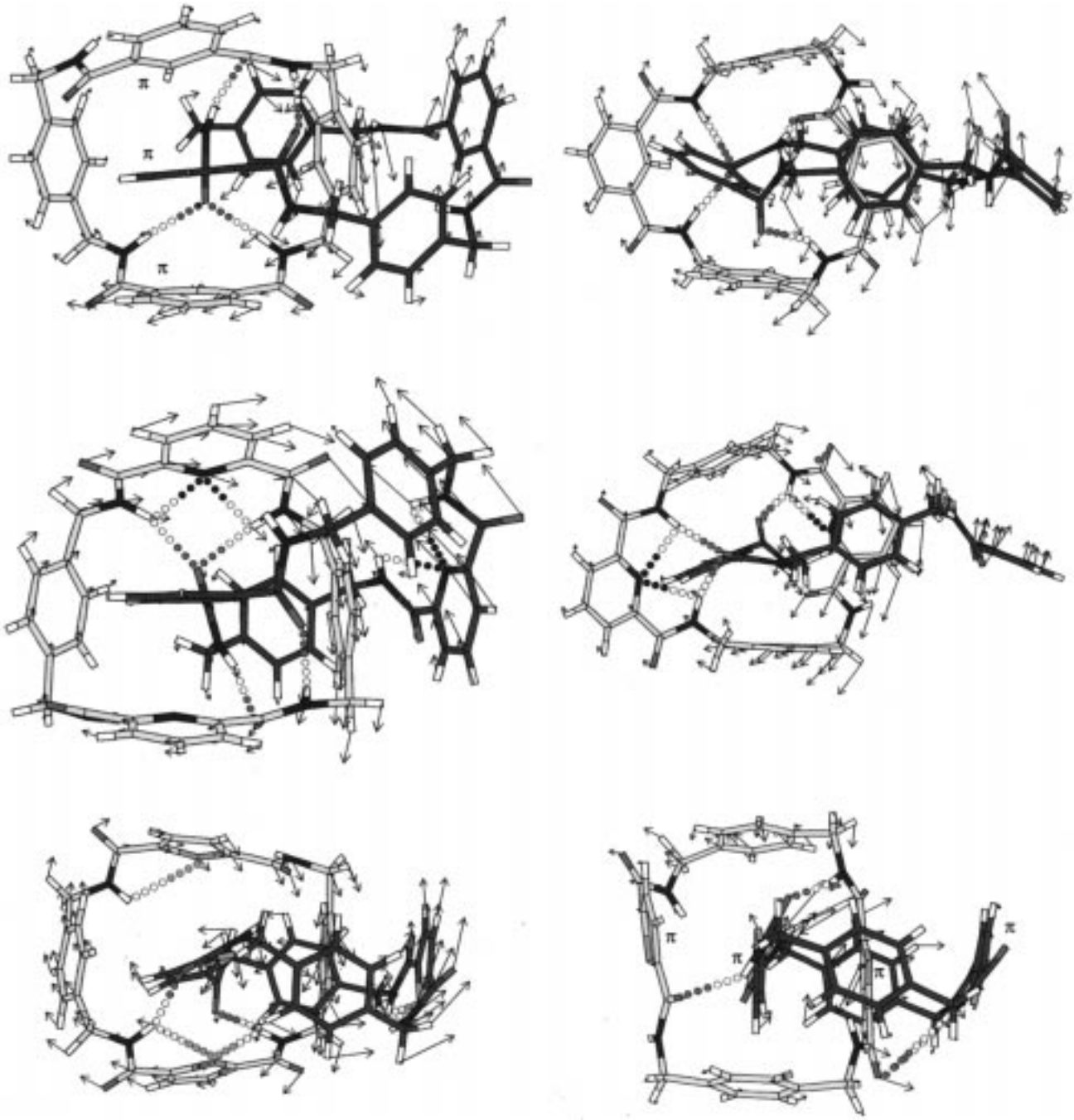

Figure 8. Catenane co-conformations and infinitesimal displacement vectors of the transition states for (a, upper left) the passing of a *p*-xylyl unit of the yellow macrocycle through the cavity of the green macrocycle in the isophthaloyl catenane (type I process in **1**); (b, upper right) the passing of an isophthaloyl unit of the yellow macrocycle through the cavity of the green macrocycle in the isophthaloyl catenane (type II process in **1**); (c, middle left) the passing of a *p*-xylyl unit of the yellow macrocycle through the cavity of the green macrocycle in the pyridyl catenane (type I process in **2**); (d, middle right) the passing of a pyridyl unit of the yellow macrocycle through the cavity of the green macrocycle in the pyridyl catenane (type II process in **2**); (e, lower left) the passing of a *p*-xylyl unit of the yellow macrocycle through the cavity of the green macrocycle in the thiophene catenane (type I process in **3**); (f, lower right) the passing of a thiophene unit of the yellow macrocycle through the cavity of the green macrocycle in the thiophene catenane (type II process in **3**). Nitrogen atoms are shown in blue; oxygen, red; hydrogen, white; and sulfur, orange.

(e.g., thiophene catenane **3** at elevated temperatures in polar solvents) to many hours to achieve a single circumrotation (e.g., pyridine catenane **2** at low temperatures in nonpolar solvents)] allowing tremendous control over the kinetics of a mechanically interlocked molecular system. A combination of NMR spectroscopy and molecular modeling explains the reasons behind this by showing that the steric effects associated with the passing of bulky groups that hinder macrocycle circumrotation are accompanied by a cascade of hydrogen bond ruptures/formations. Although these are the principal factors governing circumrotation, the negative effects of amide−amide hydrogen bond breaking are partially countered by a large number of cooperative conformational and co-conformational rearrangements that bring about the formation of multiple inter-macrocycle $\pi-\pi$ stacks, T herringbone interactions and other hydrogen bonding motifs thereby reducing key energy barriers along the circumrotational pathway and speeding up the macrocyclic ring rotation process.

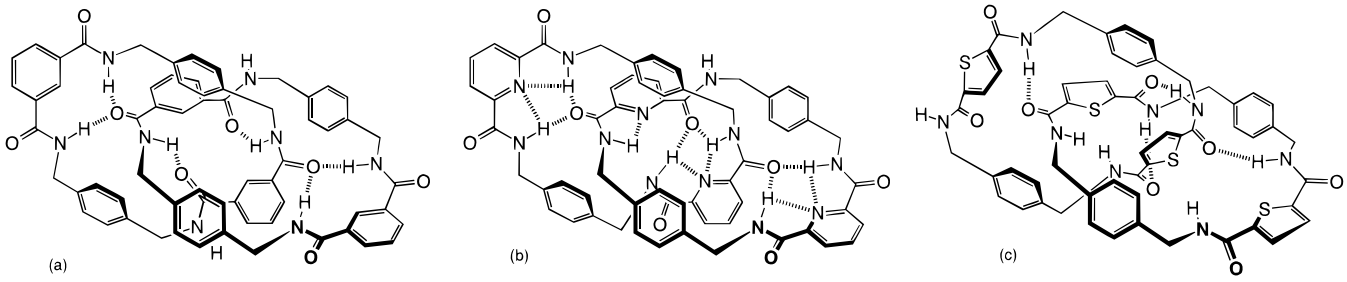

Figure 9. Low-energy hydrogen-bonding motifs for (a) **1** (taken from the X-ray crystal structure[4e]), (b) **2**, and (c) **3**.

Experimental Procedures

NMR experiments were carried out on Bruker AC300 (300 MHz) or Varian 500 (500 MHz) spectrometers (SPT-SIR experiments).

[2](1,7,14,20-tetraaza-2,6,15,19-tetraoxo-3,5,9,12,16,18,22,25-tetrabenzocyclohexacosane)-(1′,7′,14′,20′-tetraaza-2′,6′,15′,19′-tetraoxo-3′,5′,9′,12′,16′,18′,22′,25′-tetrabenzocyclohexacosane)-catenane (1).[4e] To a stirred solution of triethylamine (1.19 g, 11.8 mmol) in anhydrous (stabilized with amylenes not ethanol) chloroform (130 mL) under argon were added isophthaloyl dichloride (0.87 g, 4.3 mmol) in anhydrous chloroform (130 mL) and *p*-xylylenediamine (0.58 g, 4.3 mmol) in anhydrous chloroform (130 mL) simultaneously, over 30 min using motor-driven syringe pumps. The mixture was allowed to stir overnight and was then filtered. The filtrate was washed with 1 M aqueous hydrochloric acid (3 × 200 mL), then 5% aqueous sodium hydroxide (3 × 200 mL), and finally water (3 × 200 mL). The organic layer was then dried over anhydrous magnesium sulfate and concentrated under reduced pressure to afford 0.23 g (20.1%) of catenane (**1**). High purity material was obtained by recrystallization from dimethylformamide: mp 315 °C (decomposes); ^{1}H NMR (300 MHz, [D$_6$]DMSO) δ 8.62 (8H, s, H−d), 8.05 (4H, d, J = 1 Hz, H−c), 7.88 (8H, dd, J = 8, 1 Hz, H−b), 7.50 (4H, t, J = 8 Hz, H−a), 6.75 (16H, bs, H−f), 4.01 (16H, bs, H−e); ^{13}C NMR (75 MHz, [D$_6$]DMSO) δ 168.9, 141.3, 138.4, 133.7,132.4, 130.8, 130.0, 46.9; FAB-MS (*m*NBA matrix): *m*/*z* 1065 (M + H)$^+$, 533 (M/2 + H)$^+$. Anal. Calcd for $C_{64}H_{56}O_8N_8$: C 72.2%, H 5.3%, N 10.5%. Found C 71.9%, H 5.5%, N 9.8%.

[2](1,4,7,14,17,20-hexaaza-2,6,15,19-tetraoxo-3,5,9,12,16,18,22,25-tetrabenzocyclohexacosane)-(1′,4′,7′,14′,17′,20′-hexaaza-2′,6′,15′,19′-tetraoxo-3′,5′,9′,12′,16′,18′,22′,25′-tetrabenzocyclohexacosane)-catenane (2).[4f] To a stirred solution of triethylamine (0.40 g, 4 mmol) in anhydrous chloroform (100 mL) under argon were added pyridine-2,6-dicarbonyl chloride (204 mg, 1 mmol) in anhydrous chloroform (20 mL) and *p*-xylylenediamine (136 mg, 1 mmol) in anhydrous chloroform (20 mL) simultaneously, over 2 h using motor-driven syringe pumps. The mixture was allowed to stir overnight and was then filtered. The filtrate was washed with 1 M aqueous hydrochloric acid (3 × 60 mL), then 5% aqueous sodium hydroxide (3 × 60 mL), and finally water (3 × 60 mL). The organic layer was dried over anhydrous magnesium sulfate, concentrated under reduced pressure, and purified via column chromatography (3% MeOH in dichloromethane). The first fraction to elute was identified as the [2]catenane (**2**) (72 mg, 27%): mp 295 °C (decomposes); ^{1}H NMR (300 MHz, [D$_6$]DMSO) δ 9.28 (4H, m, H-c′), 8.79 (4H, m, H-c), 8.15−8.52 (12H, m, pyridyl), 6.88 (8H, d, J = 7 Hz, H-e′), 6.49 (8H, d, J = 7 Hz, H-e), 4.61 (8H, d, J = 5 Hz, H-d′), 3.82 (8H, d, J = 5 Hz, H-d); ^{13}C NMR (75 MHz, [D$_6$]DMSO) δ 167.8, 167.1, 153.4, 153.2, 142.3, 140.7, 132.5, 132.0, 131.7, 129.4, 129.1, 128.7, 46.6, 44.1; FAB-MS (*m*NBA matrix): *m*/*z* 1069 (M + H)$^+$, 535 (M/2 + H)$^+$. Anal. Calcd for $C_{60}H_{52}O_8N_{12}$: C 67.4%, H 4.9%, N 15.8%. Found C 67.1%, H 5.0%, N 15.3%.

[2](1,7,14,20-Tetraaza-2,6,15,19-tetraoxo-4,17-dithia-9,12,22,25-dibenzo-3,5,16,18-dicyclopentocyclohexacosane)-(4′,17′-dithia-1′,7′,-14′,20′-tetraaza-2′,6′,15′,19′-tetraoxo-9′,12′,22′,25′-dibenzo-3′,5′,16′,-18′-dicyclopentocyclohexacosane)-catenane (3).[4f] To a stirred solution of triethylamine (0.58 mL, 4 mmol) in anhydrous chloroform (100 mL) under argon were added thiophene-2,5-dicarbonyl chloride (209 mg, 1 mmol) in anhydrous chloroform (20 mL) and *p*-xylylenediamine (136 mg, 1 mmol) in anhydrous chloroform (20 mL) simultaneously, over 2 h using motor-driven syringe pumps. The mixture was allowed to stir overnight and then filtered. The filtrate was washed with 1 M aqueous hydrochloric acid (3 × 60 mL), then 5% aqueous sodium hydroxide (3 × 60 mL), and finally water (3 × 60 mL). The organic layer was then dried over anhydrous magnesium sulfate, concentrated under reduced pressure, and purified via column chromatography (3% MeOH in dichloromethane). The first fraction eluted was identified as the [2]catenane (**3**) (68 mg, 25%): ^{1}H NMR (300 MHz, [D$_6$]DMSO) δ 8.01 (8H, t, $J_{b,c}$ = 5 Hz, H-b), 7.04 (16H, s, H-d), 6.64 (8H, s, H-a), 4.15 (16H, d, J = 5 Hz, H-c); ^{13}C NMR (300 MHz, [D$_6$]DMSO) 164.7, 145.8, 142.2, 133.4, 131.7, 47.2; FABMS *m*/*z* 1089 (M + H)$^+$ and 545 (M/2 + H)$^+$. Anal. Calcd for $C_{56}H_{48}O_8N_8S_4$: C 61.8%, H 4.4%, N 10.3%, S 11.8%. Found C 61.7%, H 4.8%, N 10.2%, S 11.7%.

Acknowledgment. This work was carried out through the support of the EPSRC IPS managed program and the TMR European Network on Benzylic Amide Catenanes (ENBAC), ERB4061PL95-0968. We thank Dr Glynn J. Owen (University of Manchester) for some of the SPT-SIR measurements and Dr Frank Heatley (University of Manchester) for useful discussions.

Supporting Information Available: Cartesian coordinates of the six transition states for the three catenanes (17 pages, print/PDF). See any current masthead page for ordering information and Web access instructions.

JA974065M